Draft version April 30, 2020
Typeset using LaTeX default style in AASTeX63

Calibrating gyrochronology using Galactic kinematics

Ruth Angus,[1,2,3] Yuxi (Lucy) Lu,[3,1] Dan Foreman-Mackey,[2] Adrian M. Price-Whelan,[2] Jason Curtis,[1] and Emily Cunningham[2]

[1]*Department of Astrophysics, American Museum of Natural History, 200 Central Park West, Manhattan, NY, USA*
[2]*Center for Computational Astrophysics, Flatiron Institute, 162 5th Avenue, Manhattan, NY, USA*
[3]*Department of Astronomy, Columbia University, Manhattan, NY, USA*

ABSTRACT

Gyrochronology, the method of inferring the age of a star from its rotation period, could provide ages for billions of stars over the coming decade of time-domain astronomy. However, the gyrochronology relations remain poorly calibrated due to a lack of precise ages for old, cool main-sequence stars. Now however, with proper motion measurements from Gaia, Galactic kinematics can be used as an age proxy, and the magnetic and rotational evolution of stars can be examined in detail. We demonstrate that kinematic ages, inferred from the velocity dispersions of groups of stars, beautifully illustrate the time and mass-dependence of the gyrochronology relations. We use the kinematic ages of field stars, plus benchmark clusters and asteroseismic stars, to calibrate a new empirical Gaussian process gyrochronology relation, that fully captures the complex rotational evolution of cool dwarfs over a range of masses and ages. We use cross validation to demonstrate that this relation accurately predicts ages for GKM dwarfs.

Keywords: Stellar Rotation — Stellar Evolution — Stellar Activity — Stellar Magnetic Fields — Low Mass Stars — Solar Analogs — Milky Way Dynamics

1. INTRODUCTION

Low mass dwarfs are the most common stars in the Milky Way, and their ages could reveal the evolution of Galactic stellar populations and planetary systems. However, the ages of GKM stars are difficult to measure because their luminosities and temperatures evolve slowly on the main sequence. Fortunately, rotation-dating, or 'gyrochronology' provides a promising means to measure precise ages for these cool dwarfs. (*e.g.* Schatzman 1962; Weber & Davis 1967; Kraft 1967; Skumanich 1972; Kawaler 1988; Pinsonneault et al. 1989; Barnes 2003, 2007; Mamajek & Hillenbrand 2008; Barnes 2010; Meibom et al. 2011, 2015; van Saders et al. 2016). The rotation periods of GKM stars evolve relatively rapidly, and a fully calibrated gyrochronology model that captures the time and mass-dependence of stellar spin down could provide ages that are precise to within 20% for millions of Milky Way stars in the time-domain era (Epstein & Pinsonneault 2014; Najita et al. 2016; Angus et al. 2019). However, gyrochronology models are not yet reliably calibrated, especially for low-mass and old stars.

A lack of low-mass and old calibration stars has previously limited the mass and age coverage of gyrochronology relations, which require precise age and rotation period measurements. Historically the calibration sample has been limited to open clusters and asteroseismic stars, which can be precisely dated with isochrone fitting and main sequence turn off, or precise oscillation frequency analysis. The rotation periods of both cluster and asteroseismic stars can be measured with precise time-series photometry. Magnetically active regions create inhomogeneous surface features and produce periodic variability in their integrated, broad-band emission. The photometric rotation periods of thousands of stars have been measured with the *Kepler/K2* and *TESS* space missions (Borucki et al. 2010; Howell et al. 2014; Ricker et al. 2015).

For the purposes of calibrating gyrochronology, open clusters provide good mass coverage for young stars: rotation periods have been measured for F to mid M dwarfs up to ages of around 700 Myr. In contrast, asteroseismic stars provide reasonable age coverage for hot stars: ages and photometric surface rotation periods have been measured for F, G and early K dwarfs up to ages of 10 Gyr. However, neither asteroseismology nor cluster analysis can provide rotation periods and ages for old, late K and M dwarfs. In addition, cluster and asteroseismic stars generally provide sparse coverage of the rotation period-effective temperature plane, and cannot reveal the detailed evolution of stellar

rotation rates. As a result, most empirical gyrochronology relations are only reliable for G dwarfs up to Solar age, K dwarfs up to 2-3 Gyr, and early M dwarfs up to < 1 Gyr.

The rotational evolution of cool dwarfs is not well understood because few old M dwarfs with rotation periods have age measurements. However, as we showed in Angus *et al.* (2020), the *kinematic* ages of field stars observed by *Kepler*, can provide a calibration sample with broad mass and age coverage. Although the *Kepler* sample does not include late M dwarfs, it can still be used to extend gyrochronology relations to much older ages for late K and early M dwarfs. By adding the ages and rotation periods of thousands of field stars to the open cluster and asteroseismic calibration sample, we can calibrate a gyrochronology relation that is applicable to FGK and early M dwarfs between the ages of ∼500 Myr and 8 Gyr.

1.1. *Core-envelope decoupling*

In Angus *et al.* (2020) we demonstrated that Galactic kinematics can be used to explore the evolution of stellar rotation. We showed that velocity dispersion, an established age proxy in the Galactic thin disk, increases smoothly as a function of rotation period, indicating that rotation period increases with age as expected. Using velocity dispersion as an age proxy, we also showed that old K dwarfs spin down more slowly than G dwarfs: their rotational evolution appears to 'stall' after around 1 Gyr, in a manner that reflects the behavior of K dwarfs observed in open clusters (Curtis et al. 2019). At young ages ($\sim 0.5 - 1$ Gyr), K dwarfs spin more slowly than G dwarfs of the same age, because their deeper convection zones generate stronger magnetic fields, which leads to more efficient magnetic braking. However, at old ages ($\gtrsim 1$ Gyr) K dwarfs rotate at the same rate or more rapidly than contemporary G dwarfs. The leading explanation for this phenomenon is that angular momentum is transferred from the core to the surface over longer timescales for lower-mass stars (Spada & Lanzafame 2019), *i.e.* they experience a more extended phase of 'core-envelope decoupling'.

A period of core-envelope decoupling is necessary to explain the observed rotation periods of stars in extremely young open clusters (1-10 Gyr) (*e.g.* Irwin et al. 2007; Bouvier 2008; Denissenkov et al. 2010; Spada et al. 2011; Reiners & Mohanty 2012; Gallet & Bouvier 2013). During this phase there is little transfer of angular momentum between radiative core and convective envelope and, as wind-braking removes angular momentum from the envelope, it decelerates while the core continues to spin rapidly. Over time however, angular momentum is transported across the interface between the two zones, and momentum from the rapidly spinning interior surfaces, inhibiting the deceleration of the outer envelope. Currently, the rotation periods of field and cluster stars can only be reproduced by semi-empirical models with a mass-dependent timescale for core-envelope coupling (Spada & Lanzafame 2019; Curtis et al. 2019, Angus *et al.*, 2020).

1.2. *Using kinematics as an age proxy*

The star forming molecular gas clouds observed in the Milky Way have a low out-of-plane, or vertical, velocity (*e.g.* Stark & Brand 1989; Stark & Lee 2005; Aumer & Binney 2009; Martig et al. 2014; Aumer et al. 2016). In contrast, the vertical velocities of older stars are observed to be larger in magnitude on average (Strömberg 1946; Wielen 1977; Nordström et al. 2004; Holmberg et al. 2007, 2009; Aumer & Binney 2009; Casagrande et al. 2011; Ting & Rix 2019; Yu & Liu 2018). There are two possible explanations for this observed increase in velocity dispersion with age: either stars are born kinematically 'cool' and their orbits are heated over time via interactions with giant molecular clouds (see Sellwood 2014, for a review of secular evolution in the MW), or stars formed kinematically 'hotter' in the past (*e.g.* Bird et al. 2013). Either way, the vertical velocity dispersions of thin disk stars are observed to increase with stellar age. This behavior is codified by Age-Velocity dispersion Relations (AVRs), which typically express the relationship between age and velocity dispersion as a power law: $\sigma_v \propto t^{\beta}$, with free parameter, β (*e.g.* Holmberg et al. 2009; Yu & Liu 2018). These expressions can be used to infer the ages of groups of stars from their velocity dispersions, as we do in this paper (see section **??**).

Kinematic ages have been used to explore the evolution of cool dwarfs for over a decade. West et al. (2004, 2006) found that the fraction of magnetically active M dwarfs decreases over time, by using the vertical distances of stars from the Galactic mid-plane as an age proxy, and West et al. (2008) used kinematic ages to calculate the expected activity lifetime for M dwarfs of different spectral types. Faherty et al. (2009) used tangential velocities to infer the ages of M, L and T dwarfs, and showed that dwarfs with lower surface gravities tended to be kinematically younger, and Kiman et al. (2019) used velocity dispersion as an age proxy to explore the evolution of Hα equivalent width (a magnetic activity indicator), in M dwarfs.

AVRs are usually calibrated in Galactocentric velocity coordinates ($v_{\mathbf{x}}$, $v_{\mathbf{y}}$, $v_{\mathbf{z}}$ or UVW), and these velocities can only be calculated with full 6D positional and velocity information, however most *Kepler* rotators do not have RV measurements[1]. In Angus *et al.* (2020) we used velocity in the direction of Galactic latitude ($v_{\mathbf{b}}$) as a stand-in for $v_{\mathbf{z}}$ because, in the *Galactic* coordinate system, velocities can be calculated from 3D positions and *2D* proper motions. The *Kepler* field lies at low Galactic latitude, so $v_{\mathbf{b}}$ is a close approximation to $v_{\mathbf{z}}$. Though $v_{\mathbf{b}}$ velocity dispersion does not equal $v_{\mathbf{z}}$ velocity dispersion, it still increases monotonically over time and provides accurate age rankings for *Kepler* stars. Unfortunately however, given that AVRs are calibrated in *Galactocentric* coordinates ($v_{\mathbf{x}}$, $v_{\mathbf{y}}$, $v_{\mathbf{z}}$), we could not directly translate $v_{\mathbf{b}}$ velocity dispersions to ages.

In this paper, our aim was to use kinematic ages to calibrate a new gyrochronology relation, for which four main steps were required. Firstly, we inferred *vertical* velocity, $v_{\mathbf{z}}$, for each star without an RV measurement by marginalizing over missing RVs using a hierarchical Bayesian model (see section **??**). Secondly, we calculated velocity dispersion for every star using a moving, or rolling dispersion method (see section **??**). Thirdly, these velocity dispersions were converted into ages using an AVR (Yu & Liu 2018, section **??**). Finally, we used a Gaussian process model to capture the complexities of stellar rotational evolution and calibrated a new gyrochronology relation using our kinematic ages, plus benchmark cluster and asteroseismic stars in section **??**.

[1] Although RVs for most will be released in *Gaia* DR3

2. THE DATA

This study focuses on stellar rotation in the original *Kepler* field, partly because *Kepler* provides the largest samples of homogeneously measured rotation periods, and partly because its low Galactic latitude allows us to marginalize over missing RV measurements and precisely infer vertical velocity, $v_{\mathbf{z}}$. We combined two large rotation period catalogs constructed from original *Kepler* data: McQuillan et al. (2014) and Santos et al. (2019). These two studies used different techniques to measure rotation periods from *Kepler* light curves: autocorrelation functions and wavelets respectively. The Santos et al. (2019) study was specifically focused on cooler stars: K and M dwarfs, and includes a larger number of rotation periods for these stars. The combined catalogs provide a total of over 38,000 rotation periods.

We used the publicly available *Kepler*-*Gaia* DR2 crossmatched catalog[2] to combine the McQuillan et al. (2014) and Santos et al. (2019) rotation catalogs with the *Gaia* DR2 catalog of parallaxes, proper motions and apparent magnitudes. Reddening and extinction from dust was calculated for each star using the Bayestar dust map implemented in the `dustmaps` *Python* package (M. Green 2018), and `astropy` (Astropy Collaboration et al. 2013; Price-Whelan et al. 2018). We used *Gaia* DR2 photometric color, $G_{\rm BP} - G_{\rm RP}$, to estimate effective temperatures for the stars in our sample, using the calibrated relation in **?**.

Unlike isolated main-sequence stars, the rotation periods of binary stars and subgiants cannot always be determined by their mass and age (or at least they do not always follow the *same* gyrochronology relationship as isolated dwarfs). Photometric binaries and subgiants were therefore removed from the sample by applying cuts to the color-magnitude diagram (CMD), shown in figure **??**. A 6th-order polynomial was fit to the main sequence and raised by 0.27 dex to approximate the division between single stars and photometric binaries (shown as the curved dashed line in figure **??**). All stars above this line were removed from the sample. Potential subgiants were also removed by eliminating stars brighter than 4th absolute magnitude in *Gaia* G-band. This cut also removed a number of main sequence F stars from our sample, however these hot stars are not the focus of our gyrochronology study since their small convective zones inhibit the generation of a strong magnetic field. The removal of photometric binaries and evolved/hot stars reduced the total sample of around 38,000 stars by around 4,000.

3587 stars in our sample had RV measurements available in *Gaia* DR2, with a median uncertainty of 1.88 kms^{-1}. *Gaia* DR2 included RVs for stars with *Gaia* apparent magnitudes between around 4th and 13th, and 3550 K $\lesssim T_{\rm eff} \lesssim$ 6900 K (Gaia Collaboration et al. 2018). We also crossmatched the McQuillan et al. (2014) sample with the 5th *LAMOST* data release (Cui et al. 2012; Xiang et al. 2019), adding a further 7466 RV measurements to the sample, and expanding the total number of stars with measured RVs to 11,053. The median uncertainty of the *LAMOST* RV measurements was 4.71 kms^{-1} and, given that the *Gaia* RVs were more precise, on average, than the *LAMOST* RVs, we adopted the *Gaia* value in cases where both were available.

[2] Available at gaia-kepler.fun

3. STELLAR VELOCITIES

It has been demonstrated that the dispersion in vertical velocity, $v_{\mathbf{z}}$, of a population of stars increases with the age of that population (*e.g.* Strömberg 1946; Wielen 1977; Nordström et al. 2004; Holmberg et al. 2007, 2009; Aumer & Binney 2009; Casagrande et al. 2011; Ting & Rix 2019; Yu & Liu 2018). However, velocities in Galactocentric coordinates, $v_{\mathbf{x}}$, $v_{\mathbf{y}}$ and $v_{\mathbf{z}}$, can only be calculated with full 6-D position and velocity information, *i.e.* proper motions, position and radial velocity. In Angus *et al.* (2020) we used velocity dispersions to explore rotational evolution, however we used velocity in the direction of Galactic latitude, $v_{\mathbf{b}}$, instead of $v_{\mathbf{z}}$ because it can be calculated without an RV measurement but is a close approximation to $v_{\mathbf{z}}$ for *Kepler* stars. This is because the *Kepler* field lies at low Galactic latitudes, ($\sim 5-20°$), so the **z**-direction is similar to the **b**-direction for *Kepler* stars. However, even at such low latitudes, kinematic ages calculated with $v_{\mathbf{b}}$ instead of $v_{\mathbf{z}}$ are likely to be systematically larger because of mixing between $v_{\mathbf{z}}$, $v_{\mathbf{x}}$ and $v_{\mathbf{y}}$. A direct measurement or precise estimate of $v_{\mathbf{z}}$ is necessary to calculate accurate kinematic ages. Less than 1 in 3 stars in our sample of *Kepler* rotators had a directly measured RV available, and for these ∼11,000 stars we calculated vertical velocities, $v_{\mathbf{z}}$, using the `coordinates` library of `astropy` (Astropy Collaboration et al. 2013; Price-Whelan et al. 2018).

Although RVs were available for almost one in three stars in our *Kepler* rotation sample, few cool dwarfs had RV measurements because of the selection functions of the *Gaia* and *LAMOST* surveys. In our sample, one in 2.5 stars hotter than 5000 K had RV measurements, whereas only one in six stars cooler than 5000 K had RVs. *Gaia* DR2 only includes RVs for stars brighter than around 13th magnitude, and *LAMOST* only provides RVs for *Kepler* stars brighter than around 17th magnitude in *Gaia* *G*-band. Ruth, check the actual LAMOST selection function. Figure 1 shows the apparent magnitude and temperature distributions of the stars in our sample, with and without RVs. This figure reveals the combined selection functions of the *Gaia* DR2 and *LAMOST* RV surveys and shows that faint and cool stars have fewer RV measurements than hot, bright ones. Given that rotational evolution is particularly

Figure 1. The apparent magnitude (left) and temperature (right) distributions of stars in our sample, with and without RV measurements from *Gaia* and *LAMOST*.

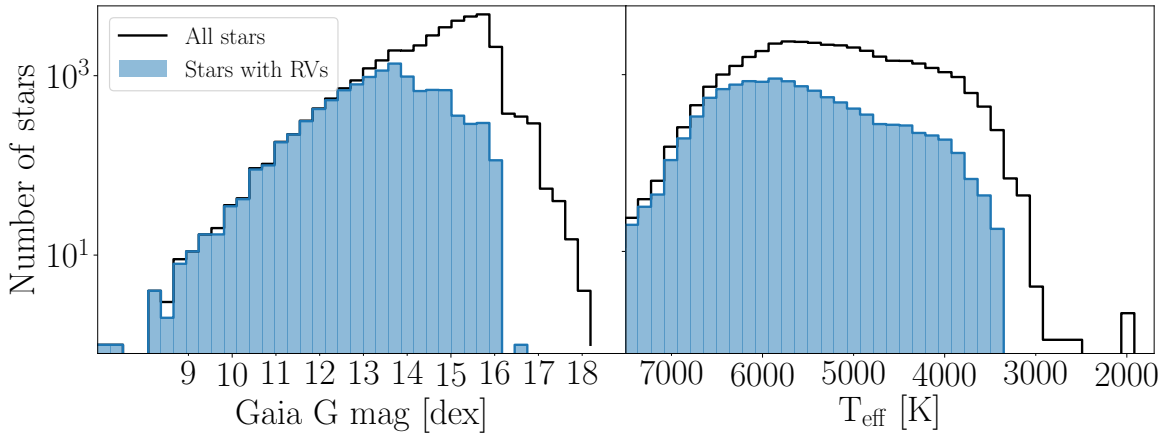

poorly understood for M dwarfs, the cool stars with missing RVs are arguably the most interesting. To fill-in the low-temperature regime, we inferred velocities for stars without RV measurements, by marginalizing over missing RVs.

3.1. *Inferring 3D velocities (marginalizing over missing RV measurements)*

For each star in our sample, we inferred $v_{\mathbf{x}}$, $v_{\mathbf{y}}$, and $v_{\mathbf{z}}$ from the 3D positions (right ascension, α, declination, δ, and parallax, π) and 2D proper motions ($\mu_\alpha$and μ_δ) provided in the *Gaia* DR2 catalog (Brown et al. 2011). We also simultaneously inferred distance, (instead of using inverse-parallax), to model velocities (see *e.g.* Bailer-Jones 2015; Bailer-Jones et al. 2018).

Using Bayes rule, the posterior probability of the parameters given the data can be written:

$$p(\mathbf{v_{xyz}}, D|\mu_\alpha, \mu_\delta, \alpha, \delta, \pi) = p(\mu_\alpha, \mu_\delta, \alpha, \delta, \pi|\mathbf{v_{xyz}}, D)p(\mathbf{v_{xyz}})p(D), \quad (1)$$

where D is distance and $\mathbf{v_{xyz}}$ is the 3D vector of velocities. To evaluate the likelihood function, our model predicted observable data from model parameters, *i.e.* it converted $v_\mathbf{x}$, $v_\mathbf{y}$ $v_\mathbf{z}$ and D to μ_α, μ_δ and π. In the first step of the model, cartesian coordinates, $\mathbf{x}$, $\mathbf{y}$, and $\mathbf{z}$ were calculated from α and δ measurements and D $(1/\pi)$ for each star, by applying a series of matrix rotations, and a translation to account for the Solar position. The cartesian Galactocentric velocity parameters, $v_\mathbf{x}$, $v_\mathbf{y}$, and $v_\mathbf{z}$, were then converted to equatorial coordinates, μ_α and μ_δ, via another rotation.

As mentioned previously, the specific positioning of the *Kepler* field (at low Galactic latitude) allows $v_\mathbf{z}$ to be well-constrained from proper motion measurements alone. This also happens to be the case for $v_\mathbf{x}$, because the direction of the *Kepler* field is almost aligned with the $\mathbf{y}$-axis of the Galactocentric coordinate system and is almost perpendicular to both the $\mathbf{x}$ and $\mathbf{z}$-axes (see figure 2). For this reason, the $\mathbf{y}$-direction is similar to the radial direction for observers near the Sun, so $v_\mathbf{y}$ will be poorly constrained for *Kepler* stars without RV measurements. On the other hand, $v_\mathbf{x}$ and $v_\mathbf{z}$ are almost perpendicular to the radial direction and can be precisely inferred with proper motions alone.

Figure 2. $\mathbf{x}$, $\mathbf{y}$ and $\mathbf{z}$ positions of stars observed by *Kepler*, showing the orientation of the *Kepler* field. The direction of the field is almost aligned with the $\mathbf{y}$-axis and almost perpendicular to the $\mathbf{x}$ and $\mathbf{z}$-axes, which is why $v_\mathbf{x}$ and $v_\mathbf{z}$ can be tightly constrained for *Kepler* stars without RVs, but $v_\mathbf{y}$ cannot.

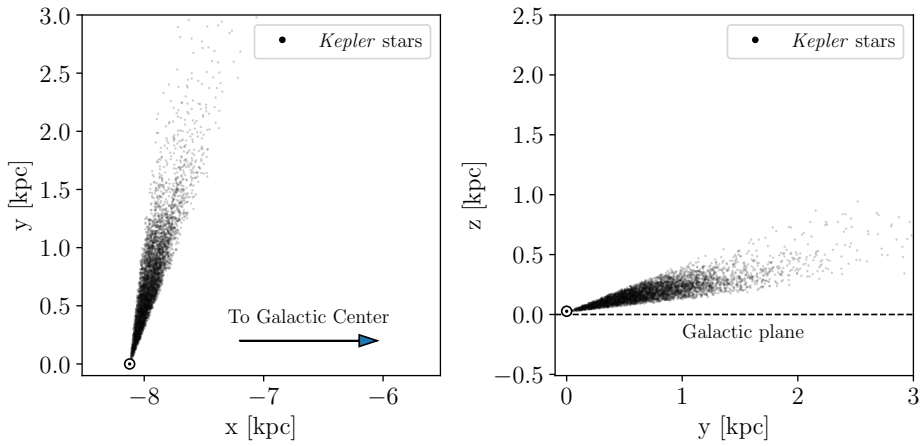

3.2. *The prior*

The prior distribution over distance and velocities was constructed from the data. We calculated the means and covariances of the $v_\mathbf{x}$, $v_\mathbf{y}$, $v_\mathbf{z}$ and $\ln(D)$ distributions of stars *with measured RVs* and then used these means and covariances to construct a multivariate Gaussian prior over the parameters for stars *without* RVs. Velocity outliers greater than 3-σ were removed before calculating the means and covariances of the distributions. The 2-dimensional log-distance and velocity distributions are displayed in figure 3, with 2-σ contours shown in blue.

Our goal was to infer the velocities of stars *without* RV measurements using a prior calculated from stars *with* RV measurements. However, stars with and without RVs are likely to be different populations, with parameters that depend on the *Gaia* and *LAMOST* selection functions. In particular, stars without RV measurements are more likely to be fainter, cooler, and further away (*e.g.* figure 1). Lower-mass stars are, on average, older, and have larger velocity dispersions, plus stars in different locations in the Galaxy have different orbital velocities. So a prior based on the velocity distributions of stars with RVs will not necessarily reflect the velocities of those without. However, given that $v_\mathbf{x}$ and $v_\mathbf{z}$ are strongly informed by proper motion measurements, and therefore likely to be relatively prior-insensitive, the prior may not impact our final vertical velocity, and subsequent kinematic ages, significantly. Remember, we are mainly interested in the $v_\mathbf{z}$ parameter because *vertical* velocity dispersion is a well-studied age indicator.

We tested the influence of the prior on the velocities we inferred. One of the main features of the *Gaia* and *LAMOST* RV selection functions is brightness: *Gaia* DR2 RVs are only available for stars brighter than around 13th magnitude, and *LAMOST* RVs for stars brighter than around 17th magnitude. Ruth, check the actual LAMOST selection function. For this reason, we tested priors based on stellar populations with different apparent magnitudes. Three priors were tested: one calculated from the velocity distributions of the brightest half of the RV sample (*Gaia* G-band apparent magnitude < 13.9), one from the faintest half ($G > 13.9$), and one from all stars with RVs. Figure 4 shows the

Figure 3. The 2D velocity and distance distributions for stars with RV measurements, used to construct a multivariate Gaussian prior over velocity and distance parameters for stars *without* RVs. 2-σ contours are shown in blue.

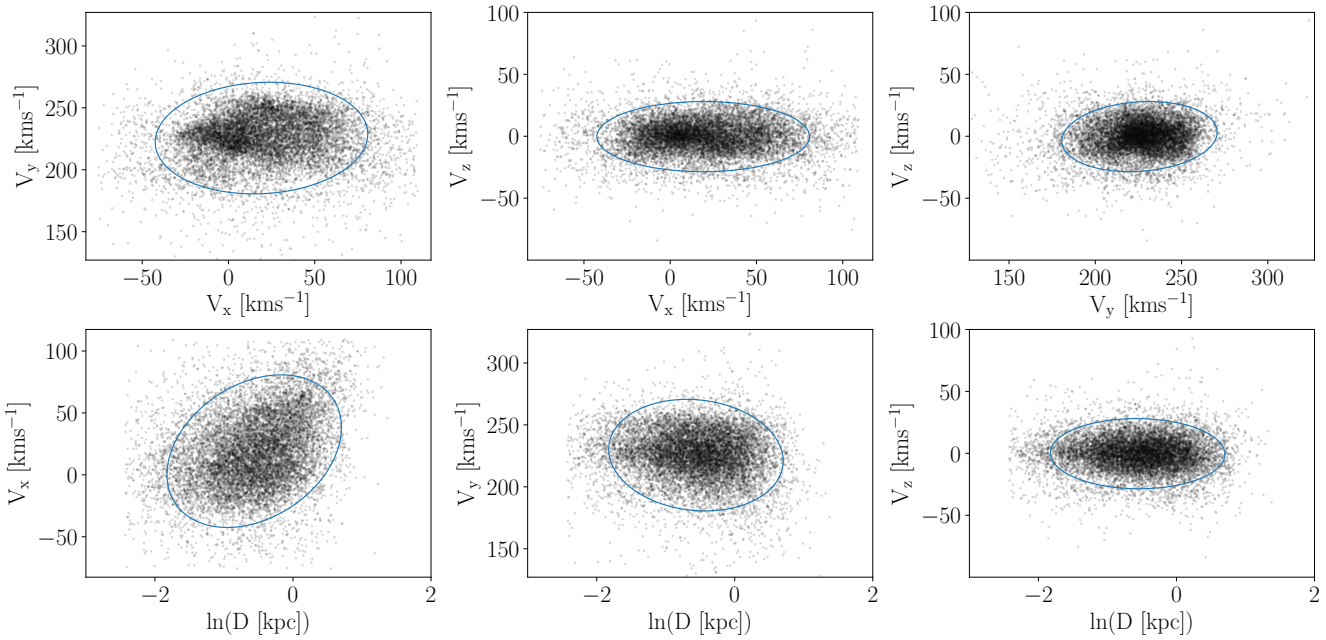

distributions of the faint (blue) and bright (orange) halves of the RV sample as kernel density estimates (KDEs). The distributions are different because bright stars are more massive, younger, and closer to the Sun on average than faint stars. As a result, these stars occupy slightly different Galactic orbits. The Gaussian fits to these distributions, which were used as prior PDFs, are shown in figure **??** as dashed, colored lines. The Gaussian fit to *all* the data, both bright and faint, is shown as a black solid line. The means of the faint and bright distributions differed by 6 kms^{-1}, 5 kms^{-1}, 1 kms^{-1} and 0.21 kpc, for $v_{\mathbf{x}}$ $v_{\mathbf{y}}$, $v_{\mathbf{z}}$ and $\ln(D)$, respectively. The $v_{\mathbf{x}}$, $v_{\mathbf{y}}$, and distance distributions of these stars are strongly dependent on brightness. However, the $v_{\mathbf{z}}$ distribution does not vary significantly with stellar brightness. Since $v_{\mathbf{z}}$ is the only velocity we actually used to infer kinematic ages, this indicates that the choice of prior does not strongly impact our final results. To confirm this, we tested the influence of the prior on the parameters.

We inferred the velocities of 3000 stars chosen at random from the *Gaia-LAMOST* RV sample using each of these three priors and compared the inferred velocity distributions. If the inferred velocities were highly prior-dependent, the resulting distributions, obtained from different priors, would look very different. The results of this test are shown in figure 5. From left to right, the three panels show the distributions of inferred $v_{\mathbf{x}}$, $v_{\mathbf{y}}$, and $v_{\mathbf{z}}$. The blue dashed line shows a KDE, representing the distributions of velocities inferred using the prior calculated from the faint half of the RV sample. Similarly, the solid orange line shows the distribution of inferred velocities using the prior calculated from the bright half of the RV sample, and the solid black line shows the results of the prior calculated from *all* stars with measured RVs.

The median values of the $v_{\mathbf{y}}$ distributions, resulting from the faint and bright priors, differ by around 4 kms^{-1}. This is similar to the difference in means of the faint and bright populations (5 kms^{-1}, as quoted above). The inferred $v_{\mathbf{x}}$ and $v_{\mathbf{z}}$ distributions differ by 2 kms^{-1} and 0.3 kms^{-1}, respectively. Regardless of the prior choice, the $v_{\mathbf{x}}$ and $v_{\mathbf{z}}$ distributions are similar because velocities in the **x** and **z**-directions are not strongly prior dependent: they are tightly constrained with proper motion measurements alone. However, the distribution of inferred $v_{\mathbf{y}}$ velocities *does* depend on the prior. This is because the **y**-direction is close to the radial direction for *Kepler* stars (see figure 2), and $v_{\mathbf{y}}$ cannot be tightly constrained without an RV measurement.

Although this test was performed on stars with RV measurements, which are brighter overall than the sample of stars without RVs (*e.g.* figure 1), figure 5 nevertheless shows that $v_{\mathbf{x}}$ and $v_{\mathbf{z}}$ are not strongly prior-dependent. In this work we are only concerned with $v_{\mathbf{z}}$, as we only use *vertical* velocity dispersion as an age indicator. The difference in the dispersions of $v_{\mathbf{z}}$ velocities, calculated with the three different priors tested above was smaller than 0.5 kms^{-1}.

Figure 4. Velocity and distance distributions of faint (blue) and bright (orange) stars with RVs, shown as KDEs. Gaussian fits to these distributions are shown as dashed lines in corresponding colors. The solid black line shows the Gaussian fit to all data (bright and faint combined) and is the prior we ended up using in our model.

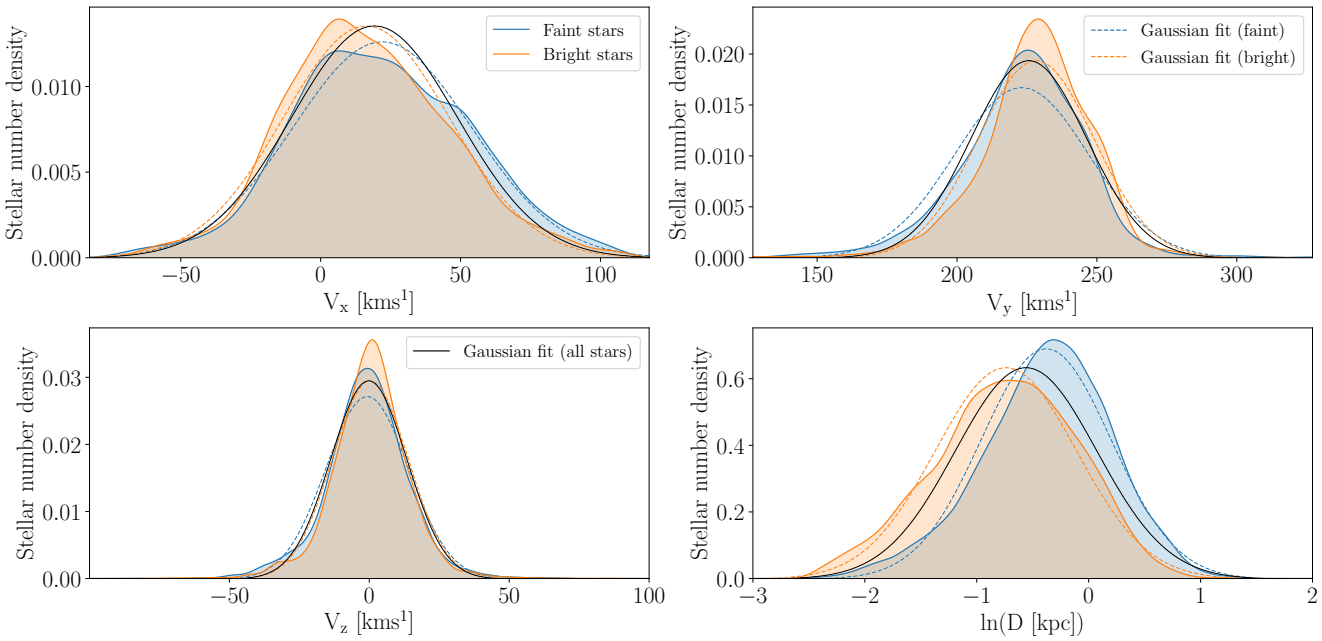

Figure 5. The distributions of velocity and distance parameters, inferred using three different priors. The orange line is a KDE that represents the distribution of parameters inferred with a Gaussian prior, estimated from the bright half of the RV sample ($G < 13.9$). The blue dashed line shows the results from a prior estimated from the faint half of the RV sample ($G > 13.9$. The black line shows the results from a prior calculated from all stars with RV measurements and is the prior we adopt in our final analysis.

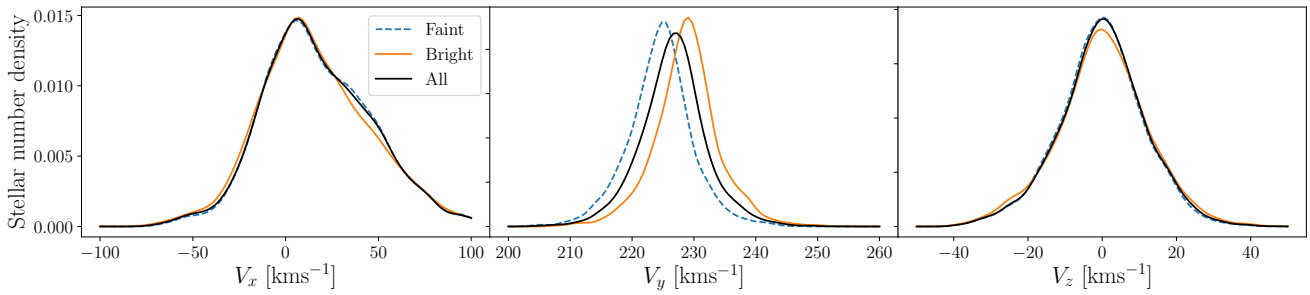

We therefore conclude that vertical velocity dispersion is relatively insensitive to prior choice, and we adopt a prior calculated from the distributions of all stars with RV measurements (black Gaussians in figure 5).

3.3. *Inferred velocities*

For each star in the *Kepler* field, we explored the posteriors of the four parameters, $v_{\mathbf{x}}$, $v_{\mathbf{y}}$, $v_{\mathbf{z}}$, and $\ln(D)$ using the *PyMC3* No U-Turn Sampler (NUTS) algorithm, and the `exoplanet` *Python* library (citations). We tuned the *PyMC3* sampler for 1500 steps, with a target acceptance fraction of 0.9, then ran four chains of 1000 steps for a total of 4000 steps. Using PyMC3 made the inference procedure exceptionally fast – taking just a few seconds per star on a laptop.

To validate our method, we inferred velocities for stars in our sample with measured RVs and compared those inferred values with velocities calculated directly from 6D position, proper motion, and RV measurements. Figure **??**

shows the $v_{\mathbf{x}}$, $v_{\mathbf{y}}$ and $v_{\mathbf{z}}$ velocities we inferred, for 3000 stars chosen at random, compared with those calculated from measured RVs.

Figure 6. Vertical velocities calculated with full 6D information vs vertical velocities inferred without RV, for 3000 McQuillan et al. (2014) stars with *Gaia* RV measurements.

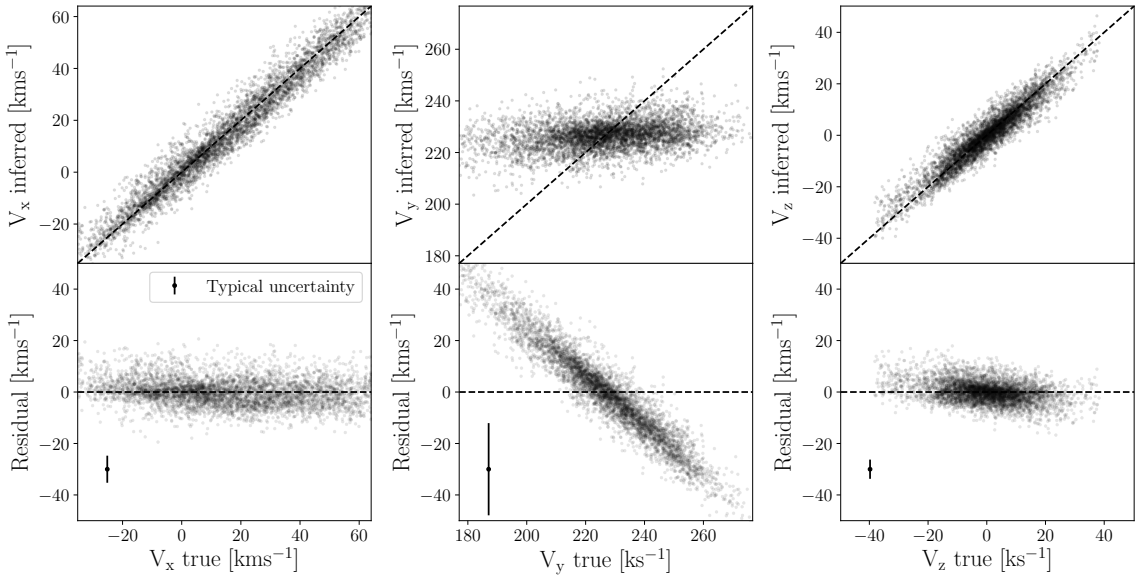

The three velocity components, $v_{\mathbf{x}}$, $v_{\mathbf{y}}$ and $v_{\mathbf{z}}$ were recovered with differing levels of precision: $v_{\mathbf{x}}$ and $v_{\mathbf{z}}$ are inferred more precisely than $v_{\mathbf{y}}$. This is because of the orientation of the *Kepler* field, shown in figure 2. Slight inaccuracies seen in the residual panels for $v_{\mathbf{x}}$ and $v_{\mathbf{z}}$ are caused by .... Quote some summary statistics.

4. KINEMATIC AGES

4.1. *Calculating velocity dispersions*

A kinematic age can be calculated from the velocity dispersion, *i.e.* standard deviation, of a group of stars. These velocity dispersions can then be converted into an age using an AVR (*e.g.* Holmberg et al. 2009; Yu & Liu 2018). Kinematic ages represent the *average age* of a group of stars and are most informative when stars are grouped by age. If a group of stars have similar ages, their kinematic age will be close the age of each individual. On the other hand, the kinematic age of a group with large age variance will not provide much information about the ages of individual stars. Velocity distributions themselves do not reveal whether a group of stars have similar or different ages, since either case the velocities are Gaussian-distributed. Fortunately however, we can group *Kepler* stars by age using the implicit assumption that underpins gyrochronology: that stars with the same rotation period and color are the same age. We discuss the implications of this assumption and cases where it doesn't apply in the Discussion of this paper (section **??**).

In this paper, we calculated the kinematic age of *each individual star* in our sample, by grouping it with its neighbors in $\log(P_{\rm rot})$–$T_{\rm eff}$ space. This method is similar to calculating a rolling, or running standard deviation and allowed us to assign a unique age to each star. However, ages calculated this way are tightly correlated, and their correlation depends strongly on window-size.

We tested two methods of grouping stars: K-nearest neighbors, and bins in $\log(P_{\rm rot})$ and $T_{\rm eff}$. In the K-nearest neighbors method, each star was grouped with the K-nearest stars in $\log(P_{\rm rot})$-$T_{\rm eff}$ space. Groups created this way spanned a small $\log(P_{\rm rot})$-$T_{\rm eff}$ range where the stellar number density was large, and a large range where the number density was small. In other words, the number of stars was fixed but the window-size changed. In the fixed range method, stars were grouped within a fixed $\log(P_{\rm rot})$-$T_{\rm eff}$window. This method created groups with large numbers of stars in densely populated regions of the $\log(P_{\rm rot})$–$T_{\rm eff}$ plane, and small numbers of stars in sparsely populated regions, *i.e.* the number of stars changed but the window-size was fixed. To choose the best method, and to optimize for the parameters of each (K and window-size), we conducted a set of tests.

4.2. *Converting velocity dispersion to age with an AVR*

We used the Yu & Liu (2018) AVR to convert velocity dispersion to age. This relation was calibrated using the ages and velocities of red clump stars. They divided their sample into metal rich and poor subsets, and calibrated separate AVRs for each, plus a global AVR. Their AVR is a power law:

$$\sigma_{vz} = \alpha t^{\beta}, \tag{2}$$

where α and β take values (6.38, 0.578) for metal rich stars (3.89, 1.01) for metal poor stars, and (5.47, 0.765) for all stars.

We used 1.5× the Median Absolute Deviation (MAD) of velocities, which is a robust approximation to the standard deviation and is less sensitive to outliers. Velocity outliers could be binary stars or could be generated by underestimated parallax or proper motion uncertainties.

4.3. *Comparing kinematic ages with asteroseismic and cluster ages*

4.4. *A Gaussian process gyrochronology relation*

5. RESULTS

6. DISCUSSION

7. CONCLUSION

This work was partly developed at the 2019 KITP conference 'Better stars, better planets'. Parts of this project are based on ideas explored at the Gaia sprints at the Flatiron Institute in New York City, 2016 and MPIA, Heidelberg, 2017. This work made use of the gaia-kepler.fun crossmatch database created by Megan Bedell.

Some of the data presented in this paper were obtained from the Mikulski Archive for Space Telescopes (MAST). STScI is operated by the Association of Universities for Research in Astronomy, Inc., under NASA contract NAS5-26555. Support for MAST for non-HST data is provided by the NASA Office of Space Science via grant NNX09AF08G and by other grants and contracts. This paper includes data collected by the Kepler mission. Funding for the *Kepler* mission is provided by the NASA Science Mission directorate.

This work has made use of data from the European Space Agency (ESA) mission *Gaia* (https://www.cosmos.esa.int/gaia), processed by the *Gaia* Data Processing and Analysis Consortium (DPAC, https://www.cosmos.esa.int/web/gaia/dpac/consortium). Funding for the DPAC has been provided by national institutions, in particular the institutions participating in the *Gaia* Multilateral Agreement.

REFERENCES

Angus, R., Morton, T. D., & Foreman-Mackey *et al*, D. 2019, AJ, 158, 173, doi: 10.3847/1538-3881/ab3c53

Astropy Collaboration, Robitaille, T. P., & Tollerud *et al*, E. J. 2013, A&A, 558, A33, doi: 10.1051/0004-6361/201322068

Aumer, M., Binney, J., & Schönrich, R. 2016, MNRAS, 462, 1697, doi: 10.1093/mnras/stw1639

Aumer, M., & Binney, J. J. 2009, MNRAS, 397, 1286, doi: 10.1111/j.1365-2966.2009.15053.x

Bailer-Jones, C. A. L. 2015, PASP, 127, 994, doi: 10.1086/683116

Bailer-Jones, C. A. L., Rybizki, J., & Fouesneau *et al*, M. 2018, AJ, 156, 58, doi: 10.3847/1538-3881/aacb21

Barnes, S. A. 2003, ApJ, 586, 464, doi: 10.1086/367639

—. 2007, ApJ, 669, 1167, doi: 10.1086/519295

—. 2010, ApJ, 722, 222, doi: 10.1088/0004-637X/722/1/222

Bird, J. C., Kazantzidis, S., & Weinberg *et al*, D. H. 2013, ApJ, 773, 43, doi: 10.1088/0004-637X/773/1/43

Borucki, W. J., Koch, D., & Basri *et al*, G. 2010, Science, 327, 977, doi: 10.1126/science.1185402

Bouvier, J. 2008, A&A, 489, L53, doi: 10.1051/0004-6361:200810574

Brown, T. M., Latham, D. W., & Everett *et al*, M. E. 2011, AJ, 142, 112, doi: 10.1088/0004-6256/142/4/112

Casagrande, L., Schönrich, R., & Asplund *et al*, M. 2011, A&A, 530, A138, doi: 10.1051/0004-6361/201016276

Cui, X.-Q., Zhao, Y.-H., & Chu *et al.*, Y.-Q. 2012, Research in Astronomy and Astrophysics, 12, 1197, doi: 10.1088/1674-4527/12/9/003

Curtis, J. L., Agüeros, M. A., & Douglas *et al*, S. 2019, arXiv e-prints. https://arxiv.org/abs/1905.06869

Denissenkov, P. A., Pinsonneault, M., & Terndrup *et al*, D. M. 2010, ApJ, 716, 1269, doi: 10.1088/0004-637X/716/2/1269

Epstein, C. R., & Pinsonneault, M. H. 2014, ApJ, 780, 159, doi: 10.1088/0004-637X/780/2/159

Faherty, J. K., Burgasser, A. J., & Cruz *et al*, K. L. 2009, AJ, 137, 1, doi: 10.1088/0004-6256/137/1/1

Gaia Collaboration, Brown, A. G. A., & Vallenari *et al.*, A. 2018, A&A, 616, A1, doi: 10.1051/0004-6361/201833051

Gallet, F., & Bouvier, J. 2013, A&A, 556, A36, doi: 10.1051/0004-6361/201321302

Holmberg, J., Nordström, B., & Andersen, J. 2007, A&A, 475, 519, doi: 10.1051/0004-6361:20077221

—. 2009, A&A, 501, 941, doi: 10.1051/0004-6361/200811191

Howell, S. B., Sobeck, C., & Haas *et al*, M. 2014, PASP, 126, 398, doi: 10.1086/676406

Irwin, J., Hodgkin, S., & Aigrain *et al*, S. 2007, MNRAS, 377, 741, doi: 10.1111/j.1365-2966.2007.11640.x

Kawaler, S. D. 1988, ApJ, 333, 236, doi: 10.1086/166740

Kiman, R., Schmidt, S. J., & Angus *et al*, R. 2019, AJ, 157, 231, doi: 10.3847/1538-3881/ab1753

Kraft, R. P. 1967, ApJ, 150, 551, doi: 10.1086/149359

M. Green, G. 2018, The Journal of Open Source Software, 3, 695, doi: 10.21105/joss.00695

Mamajek, E. E., & Hillenbrand, L. A. 2008, ApJ, 687, 1264, doi: 10.1086/591785

Martig, M., Minchev, I., & Flynn, C. 2014, MNRAS, 443, 2452, doi: 10.1093/mnras/stu1322

McQuillan, A., Mazeh, T., & Aigrain, S. 2014, ApJS, 211, 24, doi: 10.1088/0067-0049/211/2/24

Meibom, S., Barnes, S. A., & Latham *et al*, D. W. 2011, ApJL, 733, L9, doi: 10.1088/2041-8205/733/1/L9

Meibom, S., Barnes, S. A., & Platais *et al*, I. 2015, Nature, 517, 589, doi: 10.1038/nature14118

Najita, J., Willman, B., & Finkbeiner *et al*, D. P. 2016, arXiv e-prints, arXiv:1610.01661. https://arxiv.org/abs/1610.01661

Nordström, B., Mayor, M., & Andersen *et al*, J. 2004, A&A, 418, 989, doi: 10.1051/0004-6361:20035959

Pinsonneault, M. H., Kawaler, S. D., & Sofia *et al*, S. 1989, ApJ, 338, 424, doi: 10.1086/167210

Price-Whelan, A. M., Sipőcz, B. M., & Günther *et al*, H. M. 2018, AJ, 156, 123, doi: 10.3847/1538-3881/aabc4f

Reiners, A., & Mohanty, S. 2012, ApJ, 746, 43, doi: 10.1088/0004-637X/746/1/43

Ricker, G. R., Winn, J. N., & Vanderspek *et al*, R. 2015, Journal of Astronomical Telescopes, Instruments, and Systems, 1, 014003, doi: 10.1117/1.JATIS.1.1.014003

Santos, A. R. G., García, R. A., & Mathur *et al*, S. 2019, ApJS, 244, 21, doi: 10.3847/1538-4365/ab3b56

Schatzman, E. 1962, Annales d'Astrophysique, 25, 18

Sellwood, J. A. 2014, Reviews of Modern Physics, 86, 1, doi: 10.1103/RevModPhys.86.1

Skumanich, A. 1972, ApJ, 171, 565, doi: 10.1086/151310

Spada, F., & Lanzafame, A. C. 2019, arXiv e-prints, arXiv:1908.00345. https://arxiv.org/abs/1908.00345

Spada, F., Lanzafame, A. C., & Lanza *et al*, A. F. 2011, MNRAS, 416, 447, doi: 10.1111/j.1365-2966.2011.19052.x

Stark, A. A., & Brand, J. 1989, ApJ, 339, 763, doi: 10.1086/167334

Stark, A. A., & Lee, Y. 2005, ApJL, 619, L159, doi: 10.1086/427936

Strömberg, G. 1946, ApJ, 104, 12, doi: 10.1086/144830

Ting, Y.-S., & Rix, H.-W. 2019, ApJ, 878, 21, doi: 10.3847/1538-4357/ab1ea5

van Saders, J. L., Ceillier, T., & Metcalfe *et al*, T. S. 2016, Nature, 529, 181, doi: 10.1038/nature16168

Weber, E. J., & Davis, Jr., L. 1967, ApJ, 148, 217, doi: 10.1086/149138

West, A. A., Bochanski, J. J., & Hawley *et al*, S. L. 2006, AJ, 132, 2507, doi: 10.1086/508652

West, A. A., Hawley, S. L., & Bochanski *et al*, J. J. 2008, AJ, 135, 785, doi: 10.1088/0004-6256/135/3/785

West, A. A., Hawley, S. L., & Walkowicz *et al*, L. M. 2004, AJ, 128, 426, doi: 10.1086/421364

Wielen, R. 1977, A&A, 60, 263

Xiang, M., Ting, Y.-S., & Rix *et al.*, H.-W. 2019, ApJS, 245, 34, doi: 10.3847/1538-4365/ab5364

Yu, J., & Liu, C. 2018, MNRAS, 475, 1093, doi: 10.1093/mnras/stx3204